15th Australasian Wind Engineering Society Workshop
Sydney, Australia
23-24 February 2012

The Application of CFD to Modelling of Ember Attack on Houses During Bushfires

M.J. Leahy[1], K. Liow[1] and D.H. Collins[1]

[1]Synergetics Environmental Engineering, 490 Spencer St, West Melbourne, Victoria, 3003, Australia

Abstract

We describe the computational fluid dynamics (CFD) modelling of ember attack on a house. We present experimental validation of the CFD model using wind tunnel experiments of ember trajectories, finding good agreement between experiment and the CFD results. The CFD model is applied to real bushfire scenarios including internal and external flows of a house. We study the trajectory and final resting position of the embers, with a view to understand the mechanisms that cause embers to settle around a house, and ultimately improve the design of houses for bushfire conditions.

Introduction

Ember attack is the wind borne attack on a house or building by small pieces of burning wood and bark and leaf matter during a bushfire event. Ember attack is well known to be one of the most common ways a house fire occurs during a bushfire (Webster, 2008). There has been some attention given to ember attack; in particular there are studies on ember mass loss rate (Ellis, 2000; Mell 2007; CSIRO, 2000), drag properties of embers in air (Moreno et al 1965, 1967), size and mass distribution (Manzello et al 2008b), with modelling and physical experiments of ember trajectories (Anthenien, 2006; Manzello et al 2008a; Tse and Fernandez-Pello, 1998). Sharifian (2010) studied the flow through mesh screens with different mesh types – in particular to establish drag coefficient as a function of mesh porosity and single or double nature of the mesh screens. Honey et al. (2003) discussed the flow around a basic box shape building and looked at the velocity and pressure field around the house to make a link to likely ember drop out regions. Whilst this may be useful for very small embers which have a low Stokes number which are being carried along horizontally by a strong wind - and drop out when the wind approaches the low speed areas around a house - large particles take on different trajectories. In particular they will fly down in a parabolic fashion having been lifted high by thermal and mechanic forces (e.g. explosions of matter out a burning tree for example). As a result looking at the local changes in pressure and velocity in isolation is not enough to determine where embers will be likely to land. Furthermore, where embers strike a solid surface may not be the final resting place of the embers, due to the bouncing and rolling nature of embers on some solid surfaces (e.g. striking a roof and bouncing off).

The Fire Dynamics Simulator (FDS) (National Institute of Standards and Technology, 2007) has been used for micro scale modelling of fire dynamics (Sikanen, 2006; Huang et al, 2007), and this has been extended to vegetation at a larger scale by Mell et al (2007). Sikanen (2006) and Kim et al (2009) used FDS for the generation and transport of ember particles from a fire located nearby a house, and included the transport of embers from the fire front (a line of trees) to the house, and the embers landing on or inside the house. Sikanen (2006) considered the time variation of the temperature of the embers (with particle wood heat of reaction heat source) and the heat generation from the tree fire source. Huang et al (2007) considered flow, ember and thermal transport around several urban buildings. These authors modelled the embers trajectories by using the discrete phase model (DPM) CFD model - whereby the gas phase is calculated and the particle tracks are calculated based on the flow field and it is assumed that the particles do not affect the air flow hence - in a one way coupling. This approach is reasonable, however, of the studies mentioned none has looked at a refined geometry of a house and details of the bouncing behaviour, and where the embers land. In this work we have attempted to overcome this limitation.

CFD Model

For this study, the commercial all purpose solver FLUENT (ANSYS, 2011) is used to solve the proceeding steady state isothermal incompressible equations, with second order discretization schemes and the SIMPLE pressure-velocity coupling method. Turbulence modelling is handled via the Reynolds-averaged Navier-Stokes (RANS) approach, which is a good compromise of accuracy and computational efficiency. There are several approaches to modelling multiphase air-particle flows depending on the average volume fraction of particles. For dilute particle flows, the one way coupling discrete particle method (DPM) is often used. In the case of embers and air flow, it is reasonable to assume that the particles are dilute. With the DPM method, single phase air flow is calculated and the particles tracks are subsequently calculated assuming one way coupling i.e. the air flow affects the particles but not vice-versa. The particle tracks are calculated based on drag and gravity forces, and when collisions occur with walls. For the air flow model we solve the Navier-Stokes equations; the equation of continuity is given by:

$$\nabla \cdot \left(\rho_f \mathbf{v}_f \right) = 0 \tag{1}$$

and the momentum equation in steady state is given by:

$$\nabla \cdot \left(\rho_f \mathbf{v}_f \otimes \mathbf{v}_f \right) = -\nabla p' + \nabla \cdot [(\mu_f + \mu_{f,T})(\nabla \mathbf{v}_f + (\nabla \mathbf{v}_f)^T)] \tag{2}$$

where ρ_f is the air density (assumed constant), $\mathbf{v}_f$ is the air velocity, p' is the (modified) pressure (with the atmospheric reference pressure removed). The laminar viscosity is denoted μ_f (kg m^{-1} s^{-1}), and $\mu_{f,T}$ (kg m^{-1} s^{-1}) is the turbulent viscosity, described in equation (2). The turbulent viscosity $\mu_{f,T}$ in equation (2) is determined by solving transport equations for the turbulence quantities the realisable k-ε model (Shih et al, 1995) where the kinetic energy denoted k (m^2 s^{-2}) and the dissipation energy ε (m^{2}s^{-3}); it provides the most accurate description of the two equation turbulence models available for environmental flows. The realisable k-ε turbulence model has the advantage of being able to be implemented in a two or three dimensional (3D) geometry on a reasonably coarse mesh, compared to the Large-eddy simulation (LES) turbulence approach. Although the LES resolves the turbulent eddy structures more accurately, it requires significantly more computational resources than two equation turbulence models, as it needs to be solved with a fine uniform 3D mesh.

To model the embers, the following assumptions were made:

1. The forces of drag, momentum and gravity dominate the force balance.

2. Embers are considered point particles.

3. Lift and rotational motion are ignored

4. Embers do not interact with each other.

5. Embers do not have an effect on the air flow i.e. one way coupling is assumed.

The air flow described above is used as input in the following equation of motion (Huang, 2007), known as the discrete particle method (DPM):

$$m_p \frac{d\mathbf{v}_p}{dt} = V_p(\rho_p - \rho_f)\mathbf{g} + \frac{1}{2}C_D\rho_f A_p \left\|\mathbf{v}_p - \mathbf{v}_f\right\|\left(\mathbf{v}_p - \mathbf{v}_f\right) \qquad (3)$$

where the force balance terms on the right hand side of equation (3) are the gravity force and drag force respectively, and m_p and V_p are the mass and volume of the particle respectively, $\mathbf{v}_p$ is the velocity vector of the particle, ρ_p is the density of the particle, $\mathbf{g}$ (m s^{-2}) is the gravity vector, C_D is the drag coefficient and A_p is the projected area of the particle. Equation (3) is based on the particle motion of spherical particles i.e. particles of a certain diameter (or distribution of spheres with various diameters) d_{sph}. In reality the embers are non spherical, but they can be characterised to an equivalent spherical volume with diameter d_{sph}. Using this common DPM approach, embers can be assumed to be made up of a range of shapes and sizes, resembling discs and cylinders or irregular spheres, but the drag coefficient must be set according to the shape of the particles. The drag coefficient has been experimentally determined for spherical and non spherical particles by Ganser (1993) and Haider and Levenspiel (1989). These authors found good correlations with sum of squared error generally better than 98% for isometric solids like tetrahedrons etc - and as low as 90% for discs. The drag coefficient function on particle shape factor is given by:

$$C_D = \frac{24}{\mathrm{Re}\,K_1}\left[1 + 0.1118\left(\mathrm{Re}\,K_1K_2\right)^{0.6567}\right] + \frac{K_2\,0.4305}{1 + \frac{3305}{\mathrm{Re}\,K_1K_2}} \qquad (4)$$

$$K_1 = \begin{cases} \left[\frac{1}{3} + \frac{2}{3}\varphi^{-0.5}\right]^{-1} \\ \left[\frac{d_n}{3d_{eq}} + \frac{3}{3}\varphi^{-0.5}\right]^{-1} \end{cases}, \quad K_2 = 10^{1.8148(-\log\varphi)^{0.5743}} \qquad (5)$$

where φ is the particle shape factor, equal to the area of a sphere divided by the area of the particle, Re is the particle Reynolds number calculated from:

$$\mathrm{Re} = \rho_f d_{sph} V_{rel} / \mu_f \qquad (6)$$

where V_{rel} the magnitude of the relative velocity between gas and particle. Typically cylinder like particles (e.g. sticks) have particle shape factors in the range $0.6<\varphi<0.8$, and uneven but approximately sphere like particles have particle shape factors in the range $0.9<\varphi<1$.

Boundary Conditions

At all walls, no slip boundary conditions are applied, and the grid resolution is such that the normalised distance from wall to cell centre (known as Y^+) is greater than 30, and therefore in the realisable κ–ε formulation integration in the CFD solver is not carried out to the wall; instead a log profile function is used. Side and top boundaries were specified as symmetries. At the outlets a pressure boundary condition was applied and the relative pressure was set to 0Pa. Atmospheric wind speed profile is used at the inlet, where the wind speed depends on height according to

$$U = U_{ref}\left(\frac{Z}{Z_{ref}}\right)^p \qquad (7)$$

where U is the wind speed at height Z above ground, U_{ref} is the measured (or reference) wind speed at reference height Z_{ref}=10m and p is the site (and time) specific wind profile exponent. The wind profile exponent, p, is based on the Pasquill-Gifford (P-G) stability class at the specific location at a specific time We assume rural class D, with p=0.25 and U_{ref}=15m/s.

The inlet air turbulence profiles for the modelled atmospheric conditions at the inlet to the modelled domain were based on the average type of stability class identified for bushfire conditions. The realisable k-ε turbulence model requires inputs of turbulent kinetic energy, k, and turbulent dissipation rate, ε. In cases such as where the wind velocity profile is defined by a power-law as in equation 7, Richards and Hoxey (1993) recommend the use of the following expressions to define the total kinetic energy, k, and the eddy dissipation rate, ε:

$$k = \frac{u_*^2}{\sqrt{C_\mu}} \qquad (8)$$

$$\varepsilon = \frac{u_*^3}{\kappa\left(Z + Z_0\right)} \qquad (9)$$

where κ =0.4 is the von Karman constant, u_* is the friction velocity, Z_0 =0.3m is the roughness height and Z is height above ground. The total kinetic energy, k, and the eddy dissipation rate, ε, can be calculated by substituting for C_μ = 0.09 (Richards and Hoxey, 1993). The friction velocity, u*, was determined for each individual wind condition using the methods outlined in DECNSW (2005).

The embers are launched randomly from a fixed distance from the house. The bouncing of the embers is taken into consideration by the use of the coefficient-of-restitution, which reduces the embers speed as it encounters solid surfaces. This is often used to account for bouncing of particles, and is readily available for implementation in ANSYS FLUENT. The vertical and horizontal components of velocity after the collisions are described by:

$$v_{after,normal} = e_{normal} v_{before,normal} \qquad (10)$$

$$v_{after,tangent} = e_{tangent} v_{before,tangent} \qquad (11)$$

where the subscripts "before" and "after" refer to before and after the wall collision, respectively, and where e_{normal} = 0.75 and $e_{tangent}$ = 0.1 are the normal and tangent coefficients-of-restitution which have been chosen from typical values used in the literature (Kuan, 2007) for hard surfaces (like roof surface). These coefficients-of-restitution are taken to be small (e_{normal} = 0.05 and $e_{tangent}$ = 0.05) for the ground - which is assumed to be grassed, and will not readily allow embers to bounce.

Numerical Considerations

The CFD model was run in steady state using second order upwind schemes for the momentum and turbulence equations, and the SIMPLE pressure velocity coupling is used. Convergence was assumed achieved when the momentum, continuity and turbulence residuals pass below 10^{-4}. The volume mesh consisted of hexahedral elements away from the house and tetrahedral elements within a distance of 2m from the house. Inflated prismatic elements were used near the wall boundaries (for

tetrahedrons) to resolve the boundary layer regions, whilst inflated hexahedrons are used in hexahedron regions.

Experimental Validation

Experimental Setup

Manzello et al (2008a,b) conducted an experiment to establish behaviour of burning ember trajectories, using an ember generating and ejecting device - called the "Dragon" - placed in a wind tunnel under a variety of wind speeds. Machined wood particles are burned and lift off occurs at a critical size and mass when the terminal velocity is exceeded by the wind flow through the Dragon- which is set to 2m/s. The wind tunnel wind conditions are varied with speeds of 0m/s, 3m/s and 9m/s. The embers fly out and are caught in water filled pans spread out over the floor, so that they stay where they land without bouncing, allowing trajectory behaviour to be isolated. Histograms of the frequency versus distance from the Dragon exit orifice are provided, and we used these to compare with the CFD predictions. The mass and size distribution is provided, and these are used as input. Wood was machined to discs of 6mm thickness and 25mm diameter, however Manzello (2008b) states that after burning the embers broke up, and the average equivalent sphere diameter is 12mm, and has a normal distribution. We use the 0 and 9m/s cases for comparison.

0m/s Wind Tunnel Speed

Figure 1 shows the results of the CFD comparison with experimental data for the 0m/s wind speed case. There is good agreement. The embers do not travel far from the Dragon, as they are only ejected at the speed developed in the Dragon (2m/s).

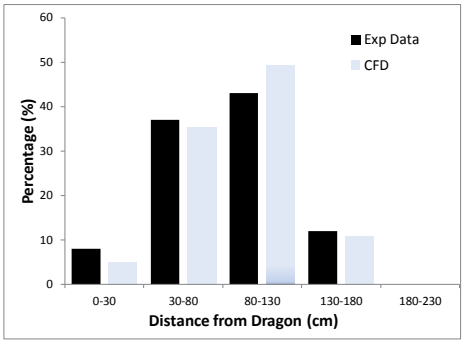

Figure 1. Histogram of distance (cm) embers land from Dragon for experimental data and CFD calculations..

9m/s Wind Tunnel Speed

At a high speed of 9m/s, the embers travel a range of 3m to 9m dragged along by the wind as shown in figure 2. There is good agreement between CFD and experimental data. This is despite the uncertainties in the shape, density, size distribution that were input in the CFD model for the particle size distribution.

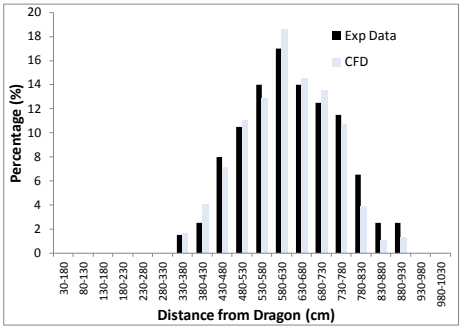

Figure 2. Histogram of distance (cm) embers land from Dragon for experimental data and CFD prediction.

Ember Attack On A House

The CFD model is applied to model the flow around and through a 10m by 10m house with veranda, deck and under-space under the deck, at U_{ref}=15m/s wind speed. The internals of the house (living space only, with no partitions) are included in the flow calculation, with entry and exit via a set of half open windows. A perspective view of the house is shown in figure 3, along with the velocity vectors - indicating the power law height profile at the inlet. Streamlines for diameters between 3 and 7mm are shown in figure 4, indicating the embers are dragged into the recirculation zone behind the house. Figure 5 and 6 show a different perspective of the embers particle tracks for a particle diameter range between 10 to 40mm and 0.1 to 0.5mm, respectively; the larger embers land on the house, veranda and veranda roof and under the veranda, whilst the smaller embers tend to fly around and over the house. No embers were observed to fly through the house, but in reality some smaller embers would be likely to. Further work would be required to ascertain why this is the case, however it may be simply that more particle tracks are required to establish representative features such as this.

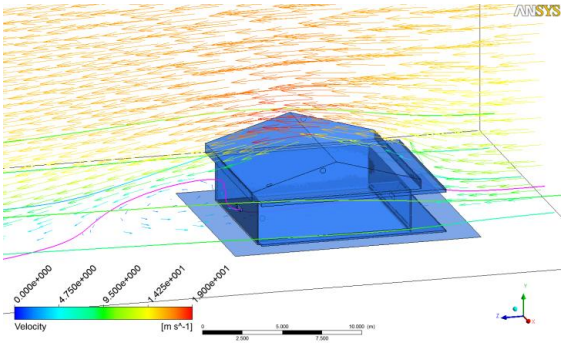

Figure 3. View of house, streamlines and velocity vector showing vertical power profile. Pink streamlines shows the flow through the house.

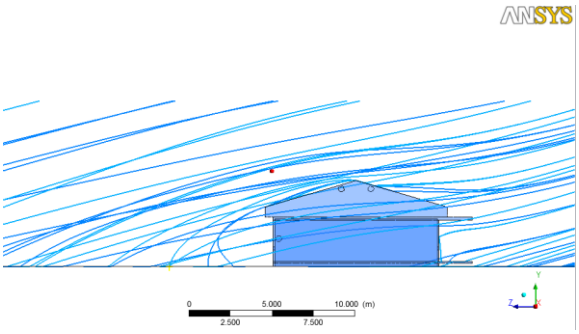

Figure 4. Particle tracks with diameters in the range 3 to 7mm. The particle are dragged into the recirculation zone behind the house.

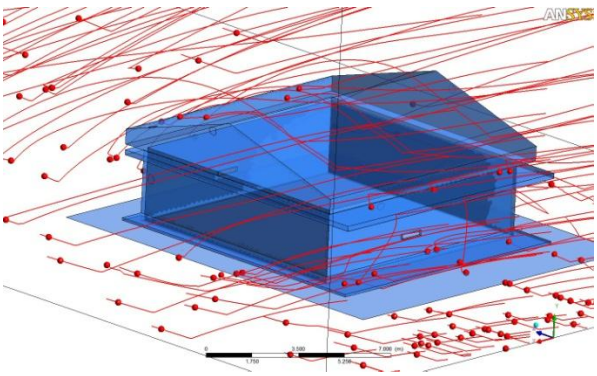

Figure 5. Particle tracks with diameters in the range 10 to 40mm.

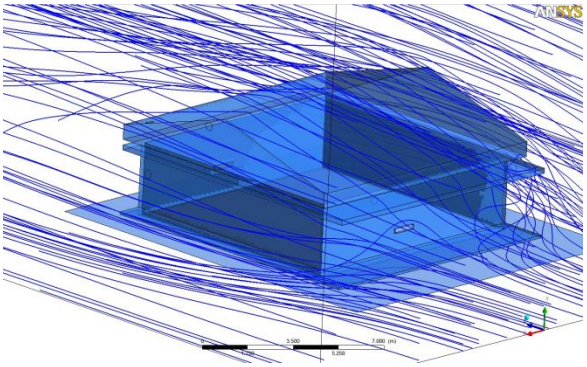

Figure 6. Particle tracks with diameters in the range 0.1 to 0.5mm.

Conclusions

This paper has discussed the CFD modelling of ember particles during bushfires, with a view to improve our understanding of the behaviour of embers and where they tend to land - either on or inside a house in a bushfire event. We showed results of the experimental validation of the CFD model, where embers were ejected from a ember chamber into a wind tunnel. The experimental data of the distance the embers landed from the chamber outlet was compared to the CFD prediction, with good agreement. The application of the CFD model to ember attack on a house was provided, showing that large embers readily land on the house, predominately the front side of the roof and flat veranda roof, whilst smaller embers flight past the house carried along by the wind. Medium sized embers land in the recirculation zone (low speed) downwind of the house.

References

ANSYS: Fluent Solver v13, ANSYS Inc., Canonsburg, USA, 2011.

Anthenien, R.A., Tse S.D. and Fernandez-Pello, A.C. (2006) On the trajectories of embers initially elevated or lofted by ground fire plumes in high winds, Fire Safety. Journal. 41: 349–363.

CSIRO 2000, http://www.csiro.au/files/mediaRelease/mr2000/spotfire.htm

DECNSW, 2005, Approved Methods for the Modelling and Assessment of Air Pollutants in New South Wales, NSW Government Gazette of 26 August 2005, Department of Environment and Conservation NSW (DEC).

Ellis, P., PhD Thesis - The aerial and combustion characteristics of Eucalypt bark - a firebrand study, Australia National University, 2000.

Ganser, G. (1993) A rational approach to drag prediction of spherical and nonspherical particles, Powder Technology, 77, 143-152.

Haider, A. and Levenspiel, O. (1989) Powder Technology, 58, 63-70.

Honey, S Rollo, J. and Atkinson, S. (2003) 2D and 3D modelling of air pressure differences and changes in wind velocity on building form subjected to ember attack,: www.urbanheart.net/Honey%20Rollo%20Atkinson%202004.pdf

Huang, H., Ooka, R., Kato, S., and Hayashi, Y. (2007) A numerical study of firebrands scattering in urban fire based on CFD and firebrands aerodynamics measurements, Journal of Fire Sciences, 25, 355-378.

Kim, Y., Hayashi, Y., Joni Tri , Y. Jeong Baek, S., (2009) A numerical study on travel distances of firebrands by wind, The Seventh Asia-Pacific Conference on Wind Engineering, November 8-12, 2009, Taipei, Taiwan.

Kuan, B, Rea, N. and Schwarz, M.P. (2007) Application of CFD in the design of a grit collection system for the coal-fired power generation industry, Powder Technology, 179: 65–72.

Manzello, S. L., Shields, J. R., Cleary, T. G., Maranghides, A., Mell, W., Yang, J. C., Hayashi, Y., Nii, D. and Kurita, T., (2008a) On the development and characterization of a firebrand generator, Fire Safety Journal, 43: 258-268.

Manzello, S. L., Cleary, T. G., Shields, J. R., Maranghides, A., Mell W. and Yang, J. C. (2008b) Experimental investigation of firebrands: Generation and ignition of fuel beds, Fire Safety Journal, 43: 226–233.

Mell, W., Jenkins, M.A., Gould, J. and Cheney, P., (2007) A physics based approach to modeling grassland fires, Internat. J.Wildland Fire, 16: 1–22.

National Institute of Standards and Technology, (2007) Gaithersburg, Maryland, USA, and VTT Technical Research Centre of Finland, Espoo, Finland. Fire Dynamics Simulator, Technical Reference Guide, 5th edition, October 2007. NIST Special Publication 1018-5 (Four volume set).

Richards, P.J., Hoxey, R.P., 1993. Appropriate boundary conditions for computational wind engineering models using the k-ε turbulence model. Journal of Wind Engineering and Industrial Aerodynamics 46 and 47, 145-153.

Sikanen, T., (2006) D2.5-4-36 Fire safety analysis around targets using FDS: Final achievements - Transport of firebrands and attack on buildings, Project no. FP6-018505.

Sharifian A. and Buttsworth, D.R., (2007) Computational Simulation of the Wind-force on Metal Meshes, 16th Australasian Fluid Mechanics Conference Crown Plaza, Gold Coast, Australia 2-7 December 2007.

Shih, T.H. Liou, W. W., Shabbir, A.,Yang, Z. and Zhu J., (1995) A New k-ε Eddy-Viscosity Model for High Reynolds Number Turbulent Flows - Model Development and Validation. Computers Fluids. 24(3). 227–238. 1995.

Tse S. D., and Fernandez-Pello, A. C., (1998) On the Flight Paths of Metal Particles and Embers Generated by Power Lines in High Winds-a Potential Source of Wildland Fires, Fire Safety Journal, 30: 333–356.

Webster, J, (2008) Essential Bushfire Safety Tips, 2nd Edition, Collingwood, CSIRO Publishing.